Since January 2020 Elsevier has created a COVID-19 resource centre with free information in English and Mandarin on the novel coronavirus COVID-19. The COVID-19 resource centre is hosted on Elsevier Connect, the company's public news and information website.

Cell Metabolism
Clinical and Translational Report

SARS-CoV-2 infects human pancreatic β cells and elicits β cell impairment

Graphical abstract

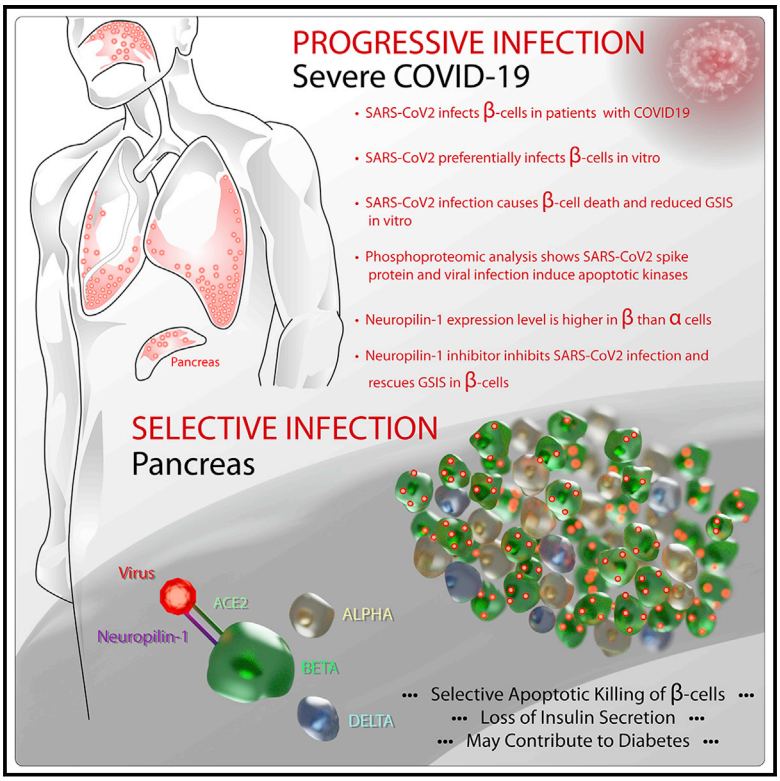

Highlights

- SARS-CoV-2 infects β cells in COVID-19 patients and human islets *in vitro*
- SARS-CoV-2 infection causes β cell death and reduced GSIS *in vitro*
- Phosphoproteomics shows SARS-CoV-2 spike protein and virus induce apoptotic kinases
- High neuropilin-1 levels support β cell selectivity, and inhibitors block infection

Authors

Chien-Ting Wu, Peter V. Lidsky, Yinghong Xiao, ..., Matthias S. Matter, Raul Andino, Peter K. Jackson

Correspondence

matthias.matter@usb.ch (M.S.M.), raul.andino@ucsf.edu (R.A.), pjackson@stanford.edu (P.K.J.)

In brief

Diabetic patients are at risk for severe COVID-19, but the virus may further damage insulin-secreting β cells. Wu et al. found that patient β cells are virally infected and the highly expressed neuropilin-1 receptor is critical for viral entry, causing cell death and reduced insulin secretion, exacerbating diabetes in patients.

Wu et al., 2021, Cell Metabolism *33*, 1565–1576
August 3, 2021
https://doi.org/10.1016/j.cmet.2021.05.013

CellPress

Cell Metabolism

CellPress

Clinical and Translational Report

SARS-CoV-2 infects human pancreatic β cells and elicits β cell impairment

Chien-Ting Wu,[1,13] Peter V. Lidsky,[2,13] Yinghong Xiao,[2,13] Ivan T. Lee,[3,4,5,13] Ran Cheng,[1,6,13] Tsuguhisa Nakayama,[5,7,13] Sizun Jiang,[3,13] Janos Demeter,[1] Romina J. Bevacqua,[8] Charles A. Chang,[8,9,10,11] Robert L. Whitener,[8] Anna K. Stalder,[12] Bokai Zhu,[3] Han Chen,[3] Yury Goltsev,[3] Alexandar Tzankov,[12] Jayakar V. Nayak,[5] Garry P. Nolan,[3] Matthias S. Matter,[12,*] Raul Andino,[2,*] and Peter K. Jackson[1,3,9,10,11,14,*]

[1]Baxter Laboratory, Department of Microbiology & Immunology, Stanford University School of Medicine, Stanford, CA 94305, USA
[2]Department of Microbiology and Immunology, University of California, San Francisco, San Francisco, CA 94158, USA
[3]Department of Pathology, Stanford University School of Medicine, Stanford, CA 94305, USA
[4]Division of Allergy, Immunology, and Rheumatology, Department of Pediatrics, Stanford University School of Medicine, Stanford, CA, USA
[5]Department of Otolaryngology-Head and Neck Surgery, Stanford University School of Medicine, Stanford, CA, USA
[6]Department of Biology, Stanford University, Stanford, CA, USA
[7]Department of Otorhinolaryngology, Jikei University School of Medicine, Tokyo, Japan
[8]Department of Developmental Biology, Stanford University School of Medicine, Stanford, CA 94305, USA
[9]Stanford Diabetes Research Center, Stanford University School of Medicine, Stanford, CA 94305, USA
[10]Stanford Cancer Institute, Stanford University School of Medicine, Stanford, CA 94305, USA
[11]Stanford ChEM-H, Stanford University, Stanford, CA 94305, USA
[12]Institute of Pathology, University of Basel, Schönbeinstrasse 40, 4003 Basel, Switzerland
[13]These authors contributed equally
[14]Lead contact
*Correspondence: matthias.matter@usb.ch (M.S.M.), raul.andino@ucsf.edu (R.A.), pjackson@stanford.edu (P.K.J.)
https://doi.org/10.1016/j.cmet.2021.05.013

SUMMARY

Emerging evidence points toward an intricate relationship between the pandemic of coronavirus disease 2019 (COVID-19) and diabetes. While preexisting diabetes is associated with severe COVID-19, it is unclear whether COVID-19 severity is a cause or consequence of diabetes. To mechanistically link COVID-19 to diabetes, we tested whether insulin-producing pancreatic β cells can be infected by SARS-CoV-2 and cause β cell depletion. We found that the SARS-CoV-2 receptor, ACE2, and related entry factors (TMPRSS2, NRP1, and TRFC) are expressed in β cells, with selectively high expression of NRP1. We discovered that SARS-CoV-2 infects human pancreatic β cells in patients who succumbed to COVID-19 and selectively infects human islet β cells *in vitro*. We demonstrated that SARS-CoV-2 infection attenuates pancreatic insulin levels and secretion and induces β cell apoptosis, each rescued by NRP1 inhibition. Phosphoproteomic pathway analysis of infected islets indicates apoptotic β cell signaling, similar to that observed in type 1 diabetes (T1D). In summary, our study shows SARS-CoV-2 can directly induce β cell killing.

INTRODUCTION

Coronavirus disease 2019 (COVID-19) is an ongoing pandemic infection caused by the positive-sense RNA virus, severe acute respiratory syndrome coronavirus 2 (SARS-CoV-2) (Zhu et al., 2020b). Although initial studies focused on lung injury and cardiovascular manifestations (Yang et al., 2020; Zheng et al., 2020), other organ dysfunctions have been observed, notably in the kidney, pancreas, intestine, and olfactory epithelia (Fang et al., 2020; Giacomelli et al., 2020; Lamers et al., 2020; Puelles et al., 2020). With regard to diabetes, several recent clinical studies suggested a significant increase in new-onset hyperglycemia, diabetic ketoacidosis (DKA), and diabetes in patients with COVID-19 (Chee et al., 2020; Ebekozien et al., 2020; Hollstein et al., 2020; Naguib et al., 2021; Rubino et al., 2020; Singh and Singh, 2020; Unsworth et al., 2020), although some studies question the statistical significance of the effect (Boddu et al., 2020). Conceptually, β cell damage could be a consequence of direct virally induced cell death or T cell autoreactivity. Therefore, the clinical association between COVID-19 and diabetes raises the first question of whether SARS-CoV-2 can infect pancreatic islet endocrine cells, particularly insulin-secreting β cells, and cause cell death or dysfunction to initiate diabetes. The binding of SARS-CoV-2 to the host cell membrane is mediated primarily by the interaction between the viral spike glycoprotein (S) and its main entry host receptor, angiotensin-converting enzyme 2 (ACE2) (Hoffmann et al., 2020). Accordingly, many recent studies have focused on analyzing the expression levels of ACE2 in pancreatic endocrine cells. Recent RNA and protein expression studies suggested low ACE2 expression levels in α, β, and δ cells

Table 1. Non-COVID-19 pancreatic tissue donor characteristics

Donor	Gender	Age	BMI	Diabetes	Cause of death	COVID-19
1	male	78	26	no	acute cardiac arrest	negative
2	male	50	29	no	advanced cancer	negative
3	male	82	18	no	left-sided cardiac failure	negative
4	female	86	24	no	combined hemorrhagic and cardiogenic shock	negative
5	male	81	28.4	no	progressing coronary insufficiency	negative

in the pancreas, leading some to postulate that SARS-CoV-2 is unable to infect β cells (Arda et al., 2016; Baron et al., 2016; Blodgett et al., 2015; Coate et al., 2020; Kusmartseva et al., 2020; Segerstolpe et al., 2016). However, these characterizations are incomplete, and a more direct evaluation of cellular SARS-CoV-2 tropism is needed. Here, we suggest that the clinical severity of diabetes in patients with COVID-19 may be notably influenced by showing direct viral infection of endocrine cells, particularly β cells.

RESULTS

Pancreatic β cells selectively express SARS-CoV-2 entry factor proteins

Recently published studies have been discordant in terms of whether the SARS-CoV-2 receptor, ACE2, is present within insulin-secreting β cells of the pancreas (Coate et al., 2020; Kusmartseva et al., 2020). While technical differences can explain the discrepancies, several of the studies found low levels of ACE2 mRNA expression in pancreatic islets, leading to speculation that SARS-CoV-2 is unable to infect β cells. However, SARS-CoV-2 entry is thought to be not only mediated by ACE2 but also by transmembrane serine protease 2 (TMPRSS2), neuropilin 1 (NRP1) (Cantuti-Castelvetri et al., 2020; Daly et al., 2020), and transferrin receptor (TFRC) (Tang et al., 2020). We first evaluated the mRNA expression level of *ACE2*, *TMPRSS2*, *NRP1*, *TFRC*, and *FURIN* in three previously published single-cell RNA sequencing (RNA-seq) datasets (Arda et al., 2016; Blodgett et al., 2015; Kim et al., 2020) in order to assess their expression within the two major pancreatic islet cell populations: insulin-secreting β cells and glucagon-secreting α cells (Figures S1A–S1C). We observed that *ACE2* and *TMPRSS2* transcripts, while expressed at low levels, are nonetheless readily measurable within both β cells and α cells. Additionally, the transcripts of other SARS-CoV-2 entry factors, *NRP1*, *TFRC*, and *FURIN*, are expressed abundantly in pancreatic islets. We next investigated the protein expression of these SARS-CoV-2 entry factors by co-staining ACE2 (Lee et al., 2020), TMPRSS2 (Suárez-Fariñas et al., 2021), NRP1 (Cantuti-Castelvetri et al., 2020; Daly et al., 2020), and TFRC (Haberger et al., 2020) in combination with insulin (INS), a β cell marker, or glucagon (GLU), an α cell marker, in pancreatic autopsy samples from 5 non-COVID-19 donors negative for COVID-19 (by PCR test). The characteristics of these donors are summarized in Table 1. Consistent with recent mRNA work, ACE2 and TMPRSS2 were generally expressed within β cells and α cells but at low protein levels (Figures 1A and S1D) (Coate et al., 2020; Kusmartseva et al., 2020). Strikingly, we found robust NRP1 and TFRC protein expression within β cells, but not α cells, suggesting a potential mechanism for SARS-CoV-2 tropism for β cells (Figures 1A and S1D). For orthogonal confirmation of this result, we utilized a different anti-NRP1 antibody to confirm the NRP1 expression in the pancreas and arrived at the same conclusion (Figure S2A). Pre-incubation of the anti-NRP1 and anti-TFRC antibodies with the immunizing peptides drastically reduced staining in the pancreas, further validating the specificity of the result (Figures S2B and S2C). To further explore this, we compared the differential protein expression of SARS-CoV-2 entry factors within β cells and α cells. Similar to the mRNA data, no major differences in ACE2 and TMPRSS2 protein expression were observed between β cells and α cells (Figure 1B), suggesting that the expression levels of these receptors are unlikely to be singularly responsible for a propensity for SARS-CoV-2 to infect β cells. Importantly, though, NRP1 and TFRC proteins were significantly increased in β cells as compared with α cells (Figure 1B). NRP1 and TFRC were recently found to facilitate ACE2-mediated SARS-CoV-2 entry (Cantuti-Castelvetri et al., 2020; Daly et al., 2020; Tang et al., 2020), whereas stable SARS-CoV-2 spike-ACE2 interactions depended on both NRP1 and TFRC. These results indicate that β cells contain the necessary molecular components for SARS-CoV-2 viral entry and that the higher expression of NRP1 and TFRC entry factors may in part explain the tropism of SARS-CoV-2 for β cells.

SARS-CoV-2 infects β cells *ex vivo* and requires NRP1

To test our hypothesis regarding the increased tropism of SARS-CoV-2 for pancreatic β cells, we isolated human islets from healthy donors and infected them with SARS-CoV-2 *ex vivo*. The characteristics of the islet donors are summarized in Table 2. Two or 6 dpi, infected pancreatic islets were fixed and stained with antibodies against the SARS-CoV-2 nucleocapsid protein (NP) in combination with antibodies against cell-type-specific markers: insulin (β cells), glucagon (α cells), somatostatin (δ cells), or CD31 (endothelial cells). Interestingly, SARS-CoV-2 NP was primarily observed in insulin-positive β cells at both 2 and 6 dpi (Figures 2A, 2C, and 2D), indicating preferential infection of β cells by SARS-CoV-2. Similar results were obtained using an antibody raised against the SARS-CoV-2 spike protein (SP) (Figures 2B–2D). In contrast, the presence of SARS-CoV-2 was notably lower in other pancreatic cell types, namely α and δ cells, and endothelial cells (Figures 2A–2D). These results strongly support the increased susceptibility of human pancreatic β cells for SARS-CoV-2.

Given the selectively high expression of NRP1 in β cells, we hypothesized that inhibition of NRP1 would be sufficient to block infection, even if other co-receptors were important. It has

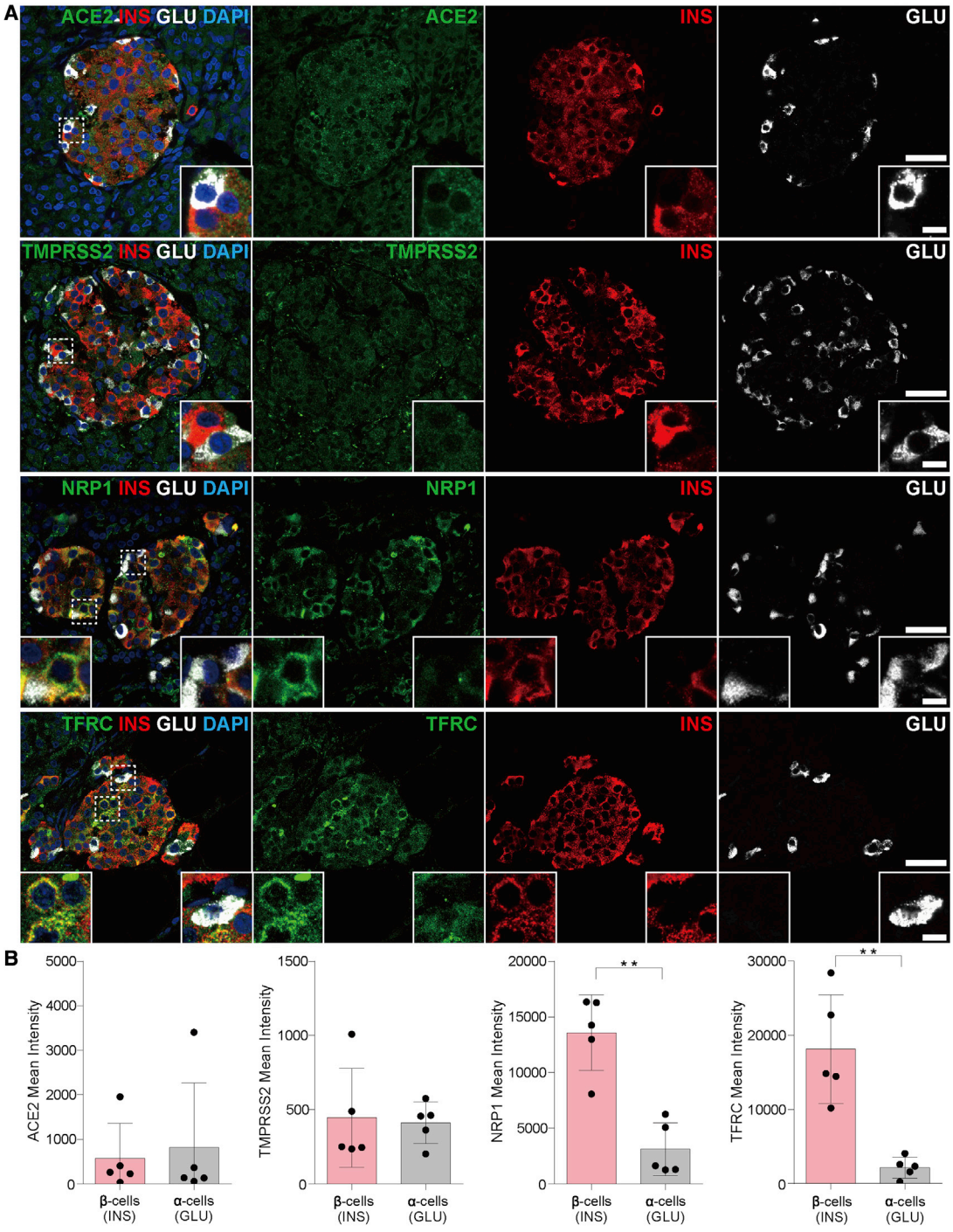

Figure 1. SARS-CoV-2-associated receptors are expressed in pancreatic β cells

(A) Representative double immunofluorescence staining of ACE2, TMPRSS2, NRP1, and TFRC with the β cell marker, insulin (INS), and α cell marker, glucagon (GLU), in the normal human pancreas, donor 1. See Table 1.

(B) Quantification of ACE2, TMPRSS2, NRP1, and TFRC in β cells (INS +) and α cells (GLU +) from a normal pancreas. No statistically significant changes in ACE2 and TMPRSS2 expression were detected between β and α cells. NRP1 and TFRC expression was statistically significantly higher in β cells compared with α cells. Rabbit anti-NRP1 (Abcam, ab81321, 1:200) and mouse anti-TFRC (Thermo Fisher, # 13-6800, 1:200) were used for the experiments shown here.

Error bars represent mean ± SD (~10–15 islets from the pancreas of 5 non-COVID-19 donors; see Table 1). **$p < 0.001$, one-way ANOVA with Tukey's post-test. Each dot represents one donor. Scale bars, 5 μm (A) and 2 μm (insets). See also Figures S1 and S2 and Table 1.

Table 2. Non-COVID-19 pancreatic islet donor characteristics

Donor	Gender	Age	BMI	Diabetes	Cause of death	COVID-19	Islet RRID
1	male	27	25.3	no	anoxia	negative	SAMN15314807
2	female	48	30.9	no	cerebrovascular/stroke	negative	SAMN15770453
3	male	52	24.5	no	cerebrovascular/stroke	negative	SAMN15850322
4	female	63	26.9	no	cerebrovascular/stroke	negative	SAMN15942269
5	male	35	31.3	no	head trauma	negative	SAMN16191825
6	female	42	31.2	no	cerebrovascular/stroke	negative	SAMN16427178
7	female	51	25.2	no	cerebrovascular/stroke	negative	SAMN16515959
8	male	37	25	no	head trauma	negative	UNOS ID: AHJX486
9	female	53	27.4	no	cerebrovascular/stroke	negative	UNOS ID: AHK2444
10	male	60	29.9	no	anoxia	negative	SAMN17528599
11	female	44	23.8	no	cerebrovascular/stroke	negative	UNOS ID: AIA3480
12	male	62	25.9	no	head trauma	negative	SAMN17928660
13	male	56	24.2	no	anoxia	negative	SAMN18021384

been shown that the treatment of the small molecule EG00229, a selective NRP1 antagonist, reduced the efficiency of SARS-CoV-2 infection *in vitro* (Daly et al., 2020). Here, we also found that incubation of *ex vivo* pancreatic islets with EG00229 notably reduced the efficiency of SARS-CoV-2 infection (Figure 2E). This result supports a critical role of NRP1 protein in the increased tropism of SARS-CoV-2 for pancreatic β cells. Additional studies will be needed to further establish the relationship between levels of NRP1 and the levels of other viral receptors and the efficiency of infection.

SARS-CoV-2 infects β cells in subjects with COVID-19

Next, we determined whether SARS-CoV-2 tropism for β cells is also observed in patients with COVID-19. We obtained pancreatic autopsy samples from 9 patients who died from severe COVID-19-related complications. The characteristics of these patients are summarized in Table 3. Histological analysis revealed lipomatosis, fibrosis, or autolysis in some of the samples, whereas acute or chronic pancreatitis was not observed in any patient (Table 1), tending to exclude that broad pancreatic damage is a universal feature. The pancreas of 7 out of 9 of these patients had SARS-CoV-2 viral positivity as measured by RT-PCR. We observed SARS-CoV-2 NP staining selective to insulin-positive β cells in 4 of 7 patients, while the remaining 3 pancreatic samples and healthy control samples were negative for NP staining (Figure 3A). The specificity of the anti-NP antibody was validated through peptide blocking assays (Figure S2D). The 3 negative samples (staining not shown) from patients with COVID-19 had extensive autolysis/atrophy (Table 3), which may explain the lack of NP signal due to rapid proteolysis of tissue by digestive enzymes. As an orthogonal confirmation of our observations of viral presence in β cells, we performed *in situ* hybridization (ISH) using a validated SARS-CoV-2 spike mRNA probe in combination with an antibody targeting insulin on the four positive SARS-CoV-2-infected human pancreatic tissues (see Figures S3A and S3B for SARS-CoV-2 probe validation) (Lee et al., 2020). Similar to the NP staining results, SARS-CoV-2 spike transcripts were detected in β cells of these autopsied pancreatic islets (Figure 3B). These results confirm SARS-CoV-2 tropism for β cells, supporting a model in which SARS-CoV-2 infects and replicates in β cells to induce pancreatic dysfunction, thus leading to hyperglycemia or diabetes.

We next investigated whether ACE2 and NRP1 are differentially expressed in the pancreatic β cells of patients with COVID-19 compared with non-COVID-19 donors as a potential explanation for why β cells are more susceptible to viral infection. ACE2 expression remained low in individuals with COVID-19 with no statistically significant difference compared with non-COVID-19 donors (Figures S3C and S3D). Conversely, NRP1 expression is upregulated in patients with COVID-19 compared with non-COVID-19 donors (Figures S3C and S3D). These results support a potential role of NRP1 in β cell susceptibility of viral infection. However, it is also possible that this is due to the increased NRP1 expression in the organ caused by SARS-CoV-2 infection, which in turn causes the cells to be more susceptible to infection. Further research is needed to establish the generality and mechanism by which SARS-CoV-2 may require either (1) preexisting or (2) virally induced upregulation of NRP1 levels.

SARS-CoV-2 infection suppresses insulin secretion and kills β cells *ex vivo*

To determine whether SARS-CoV-2 infection affected pancreatic islet function, we quantified the insulin content and glucose-stimulated insulin secretion (GSIS), a functional assay for β cell insulin release, in infected islets. We observed a dramatic decrease in insulin content and GSIS in SARS-CoV-2-infected human islets, compared with mock-treated islets (Figures 4A and 4B). Notably, this effect is partially reversed upon treatment with the NRP1 antagonist EG00229 (Figure S3E). In type 1 diabetes (T1D), virus-induced β cell damage can be a result of either virus-triggered cell death or immune-mediated loss of infected pancreatic β cell mass. Previous reports of SARS-CoV-1/2-induced apoptosis in ACE2-expressing A549 and Vero E6 cells (Diemer et al., 2008; Li et al., 2020; Zhu et al., 2020a) suggested a similar mechanism of virus-mediated cell death in pancreatic β cells *ex vivo*. To this end, we performed the terminal deoxynucleotidyl transferase dUTP nick end labeling (TUNEL) assay on SARS-CoV-2-infected human islets 6 dpi. TUNEL signal was significantly increased in infected β cells,

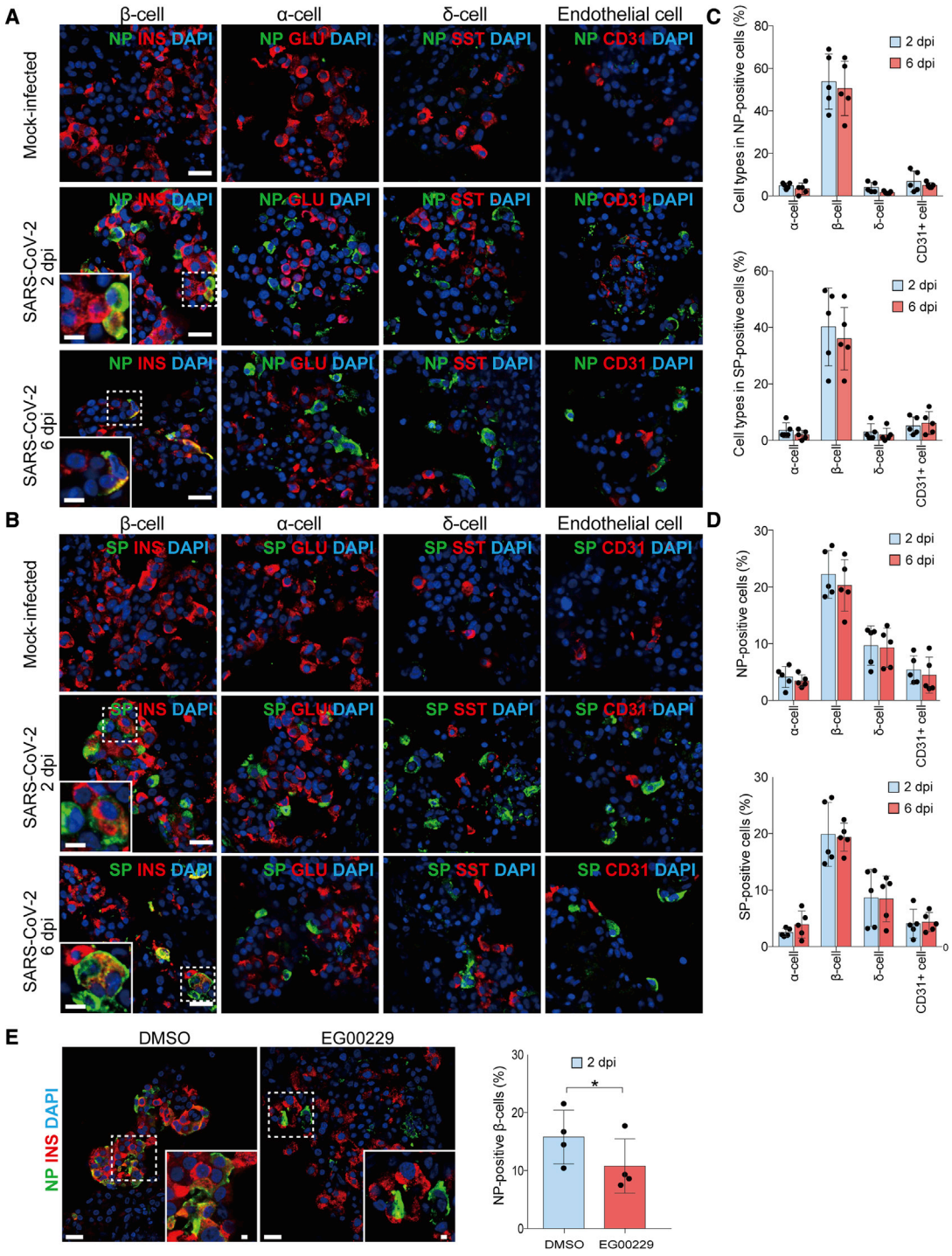

Figure 2. SARS-CoV-2 preferentially infects β cells of human pancreatic islets *ex vivo*

(A–D) Mock-treated or SARS-CoV-2-infected human pancreatic islets were stained after 2 or 6 dpi. (A) Representative double immunofluorescence staining of SARS-CoV-2 nucleocapsid protein (NP) in combination with β cell marker, insulin (INS); α cell marker, glucagon (GLU); δ cell marker, somatostatin (SST); and endothelial cell marker (CD31).

(B) Representative double immunofluorescence staining of SARS-CoV-2 spike protein (SP) in combination with a similar combination of markers as (A). The nuclei were stained using DAPI (blue) as a counterstain.

(C) Quantified percentages of SARS-CoV-2 NP and SP within α, β, δ, and endothelial cells of pancreatic islets. Around 40% to 60% NP and SP staining, respectively, are present within β cells.

(D) Quantified percentages of SARS-CoV-2 NP- and SP-positive α, β, δ, and endothelial cells.

(C and D) Error bars represent mean ± SD (~500–1,000 cells were quantified from healthy isolated human islets from donors 1–5; see Table 2).

(legend continued on next page)

compared with mock-infected β cells (Figures 4C and 4D). Since SARS-CoV-2 also infects a small number of other cells, such as α cells, a population that accounts for the second-largest number of cells in the islet, we next investigated whether SARS-CoV-2 infection can cause apoptosis of α cells (Figure S3F). The increased TUNEL signal in infected α cells suggests that viral infection-induced cell death was agnostic to cell type, although the percentage of β cells undergoing apoptosis was higher due to higher susceptibility. SARS-CoV-2 spike protein treatment was sufficient to induce apoptosis in β cells, as indicated by an increase in TUNEL signal (Figures 4E and 4F). This observation is consistent with past findings that SARS-CoV-1 SP can induce apoptosis in Vero E6 cells (Chow et al., 2005). Altogether, these results support a model in which SARS-CoV-2-induced β cell apoptosis leads to dysregulation in insulin production and secretion.

Given the central role of regulatory kinases in the control of apoptosis, we next asked whether the binding of SARS-CoV-2 to its receptors is sufficient to trigger apoptosis-related signaling pathways independent of additional cellular stress as a result of viral infection and replication. We first leveraged assaying global phosphoproteomics to determine potential kinase regulatory roles of the SARS-CoV-2 SP, which directly binds the viral receptors. Isolated human islets were incubated with SARS-CoV-2 SP from SARS-CoV-2 for 15 or 30 min in parallel with vehicle control treatment. Cells were then harvested, and extracts were prepared for phosphoproteomic mass spectrometry and analysis of signaling (Figure S4A). We employed a substrate-based kinase activity prediction model to determine the activity levels of specific kinases from this large-scale phosphoproteomic data. This analysis is based on the underlying assumption that the activity levels of upstream kinases can be inferred through the measured abundance of known downstream target phosphorylation events (Hernandez-Armenta et al., 2017). Using kinase set enrichment analysis (KSEA) (Drake et al., 2012; Ochoa et al., 2016), we were able to assign an enrichment score (ES) value (weighted Kolmogorov-Smirnov statistic; STAR Methods) to each kinase to reflect its activity in a manner analogous to that of gene set enrichment analysis (GSEA) (Subramanian et al., 2005). Differential expression of phosphosites in the 15- and 30-min SARS-CoV-2 SP-treated human islets was calculated by comparing them to vehicle control, and KSEA was performed using a kinase-substrate database created using PhosphoSitePlus (Hornbeck et al., 2015) and NetworKin (Linding et al., 2008).

Quantification of the activity of 67 kinases (Figure S4B; Tables S1 and S2) revealed an upregulation of stress-response MAP kinases, including JNK/p38 (MAPK8/11) (Wada and Penninger, 2004) and cytoskeleton reorganizing p21-activated kinases (PAK) (Manser et al., 1994), which are two classic pathways triggering cell death by the apoptosis pathways. Additionally, multiple members of the protein kinase C (PKC) family were downregulated in response to SARS-CoV-2 SP treatment. Through pathway analysis using gene ontology (GO) biological process over-representation analysis (ORA), apoptosis emerged as a recurring top hit (Figures S4C and S5A–S5D; Table S3) as early as 30 min post-SARS-CoV-2 spike protein incubation. Apoptotic kinases, including PAK, were upregulated, as was activation of GSK3β and the proapoptotic kinase JNK1, both previously linked to apoptosis in β cells (Dhanasekaran and Reddy, 2008; Guo et al., 2016; Tournier et al., 2000) (Figures S5E–S5I).

To understand whether the same pathways were activated by a viral infection, we repeated the phosphoproteomics analysis on cells infected with SARS-CoV-2 (24 h post-infection) to measure the activity levels of specific kinases triggered by the virus. As with SARS-CoV-2 SP treatment, we also observed upregulation of JNK and PAK in SARS-CoV-2-infected islet cells (Figure S4B). As before, GO analysis pointed to apoptosis and programmed cell death as the most significantly enriched categories (Figure S4D). To validate that JNK and PAK are indeed activated in virus-infected islets, we co-stained phosphorylated JNK1/2 (pJNK1/2) and phosphorylated PAK1/2 (pPAK1/2) in combination with the SARS-CoV-2 SP in infected pancreatic islets. Our results confirm that pJNK1/2 and pPAK1/2 were primarily observed in SARS-CoV-2 SP-positive cells at 24 h post-infection (Figure S4E), confirming that the SARS-CoV-2 infection induces the activation of JNK and PAK. The kinase activities induced by SARS-CoV-2 SP and SARS-CoV-2 infection support a mechanism through which SARS-CoV-2 induces apoptosis via the JNK-MAPK apoptosis pathway, allowing a potential window for therapeutic intervention.

DISCUSSION

Emerging clinical reports have noted a significant increase in new-onset hyperglycemia, DKA, and diabetes in patients with COVID-19. Understanding how SARS-CoV-2 affects the normal function of the pancreas is an urgent unmet need with fundamental healthcare implications. In this study, we discovered that SARS-CoV-2 preferentially infects β cells in isolated human pancreatic islets *ex vivo* and in patients who succumbed to COVID-19. Building on recent studies that identified low-level ACE2 expression in pancreatic islets (Fignani et al., 2020; Kusmartseva et al., 2020), we observed that ACE2 as well as TMPRSS2 are indeed modestly expressed in β cells. Importantly, we uncover the selective expression of other critical SARS-CoV-2 entry factors, NRP1 and TFRC, in β cells. We propose that this enrichment of NRP1, and possibly TFRC, is a potential mechanism underlying SARS-CoV-2 tropism for β cells. Further studies incorporating more robust reagents, such as well-validated antibodies, will be needed to better understand the additional roles of other factors implicated in SARS-CoV-2 entry, including TMPRSS4, Furin, and heparan sulfate (Clausen et al., 2020). Heparan sulfate, in particular, has been shown to be highly expressed in pancreatic β cells and plays an important

(E) Representative double immunofluorescence staining of SARS-CoV-2 NP in combination with insulin after pre-treating islets with dimethyl sulfoxide (DMSO) or 100 μM EG00229 for 1 h before infection with SARS-CoV-2. Islets were fixed at 2 dpi and stained for SARS-CoV-2 NP and β cell marker, insulin (INS). Quantification of the percentages of β cells containing NP-positive β cells (right).

Error bars represent mean ± SD (~500–1,000 cells were quantified from healthy isolated human islets from donors 10–13; see Table 2). *$p < 0.05$, two-tailed Student's t test. Each dot represents one donor. Scale bars, 5 μm (A, B, and E) and 2 μm (insets). See also Table 2.

Table 3. COVID-19 patient characteristics, pancreas viral load, percentage of NP+ islets, and histological analysis

Patient	Age	BMI	Diabetes	Viral load PCR (mean)	Ct values (ORF, S, N)	NP-positive islets (%)	Histological analysis
1	67	35	no	29	33/32/35	4	well preserved, mild fibrosis
2	85	26	type II	108	35/35/35	31	mild fibrosis, lipomatosis, and autolysis
3	95	23	no	24	34/33/33	5	well preserved, lipomatosis, and mild fibrosis
4	71	24	no	15	35/35/indet	12	mild lipomatosis and autolysis
5	88	28	no	6	31/32/32	0	extensive atrophy, lipomatosis, and moderate fibrosis
6	85	30	no	11	38/37/36	0	extensive autolysis
7	58	47	no	16	38/35/36	0	extensive autolysis
8	66	29	no	indeterminate	indeterminate	0	mild lipomatosis, fibrosis, autolysis
9	54	30	no	indeterminate	indeterminate	0	extensive autolysis

Pancreatic autopsies were obtained from 9 patients who died from COVID-19-related complications. The pancreas of 7 out of 9 of these patients had SARS-CoV-2 viral positivity by RT-PCR. Ct values of RT-PCR targeting three different SARS-CoV-2 genomic regions (ORF1ab, spike [S], and nucleocapsid [N]) are shown. Ct values of the pancreas from patients 8 and 9 were between 37 and 40 and therefore considered "indeterminate" and not positive. The percentages of the nucleocapsid (NP)-positive islets by immunofluorescence staining as described in the manuscript are also shown for each patient sample. Pancreas from patients 5–7 did not have NP positivity, possibly due to extensive autolysis/atrophy. Histological analysis was performed by a board-certified pathologist (M.S.M.).

role in regulating β cell survival (Simeonovic et al., 2018; Ziolkowski et al., 2012) and would be another leading candidate in determining SARS-CoV-2 tropism for β cells.

Of note, while we found SARS-CoV-2 localization within β cells from 4 autopsied patients, SARS-CoV-2 NP was not detected in pancreatic islets from 3 autopsied patient samples from a separate report (Kusmartseva et al., 2020). This discrepancy is likely due to the issue that pancreatic tissues are highly prone to autolysis, resulting in the rapid proteolysis of proteins due to the abundance of digestive enzymes. Indeed, we also did not detect SARS-CoV-2 NP signal in 3 out of 7 pancreas tissues with extensive pathologist-verified autolysis/atrophy, further suggesting the importance of rapid tissue preservation and documentation during COVID-19 autopsies. For these samples, we were able to confirm viral genomic expression by ISH in β cells as evidence of viral infection. Finally, we showed that SARS-CoV-2 infection leads to dysregulation of insulin homeostasis, induction of apoptosis-associated signaling pathways, along with cell apoptosis, mainly in β cells. These key observations support a mechanism through which SARS-CoV-2 can directly drive β cell damage to cause clinical T1D linked to hyperglycemia. These effects of the virus are not mutually exclusive with the possibility that SARS-CoV-2 can also induce autoimmune-mediated β cell destruction and is the subject of further investigation. Nonetheless, at least our microscopic histological observations do not suggest ongoing insulitis. Additional limitations of our study are the small sample size of pancreas samples from patients with COVID-19 and the lack of pancreas from children due to challenges in procuring these tissues. Moreover, since we utilized the pancreas from patients who succumbed to severe COVID-19, we are unable to generalize the SARS-CoV-2 β cell tropism to all patients with COVID-19, particularly those with mild COVID-19 due to the invasiveness of such a biopsy. Indeed, only a minority of patients with COVID-19 develop hyperglycemia, DKA, or T1D (Chee et al., 2020; Ebekozien et al., 2020; Hollstein et al., 2020; Naguib et al., 2021; Rubino et al., 2020; Singh and Singh, 2020; Unsworth et al., 2020).

Although we identify a mechanism explaining β cell-selective cell death, many details of how the virus migrates to the pancreas in patients with severe COVID-19 remain unclear. We suspect that following the initial infection of the upper airway and secondary expansion of the virus to the lungs, viral particles can be taken up by the vasculature and propagated to vascularized organs including the pancreas, kidney, and brain. From there, the route of vascular exit and viral entry to the tissue itself may require additional steps or preconditions to favor viral attack of secondary tissues like the pancreas. It would be of value to evaluate patient records to determine the time of onset of COVID-19-induced pneumonia, marking severe lung infection, compared with the evolution of hyperglycemia as a marker of pancreatic damage and a diabetes-like effect on insulin secretion.

While this manuscript was under review, Müller and colleagues (Ulm University Medical Center, Germany) reported that SARS-CoV-2 infects human pancreatic endocrine cells *ex vivo* and *in vivo* and interferes with β cell functions *ex vivo* (Müller et al., 2021). While the general findings are similar to ours, there are some important key discrepancies. First, inconsistent with previous studies, these authors found that ACE2 and TMPRSS2 expression are higher in β cells than α and δ cells. We and others found that ACE2 and TMPRSS2 expression are low in islets (Figure 1) (Coate et al., 2020; Kusmartseva et al., 2020) both at the mRNA and protein levels. Furthermore, we identified the expression of two other SARS-CoV-2 entry receptors, NRP1 and TFRC, to be higher in β cells than α cells (Figure 1). NRP1 expression, and not ACE2, was found to be upregulated in patients with COVID-19 compared with non-COVID-19 donors (Figure S3). Treatment of human islets with an NRP1 inhibitor reduces infection by SARS-CoV-2 and partially rescues GSIS in the islets, showing the critical role of NRP1 for enabling SARS-CoV-2 infection. Second, although the authors confirmed

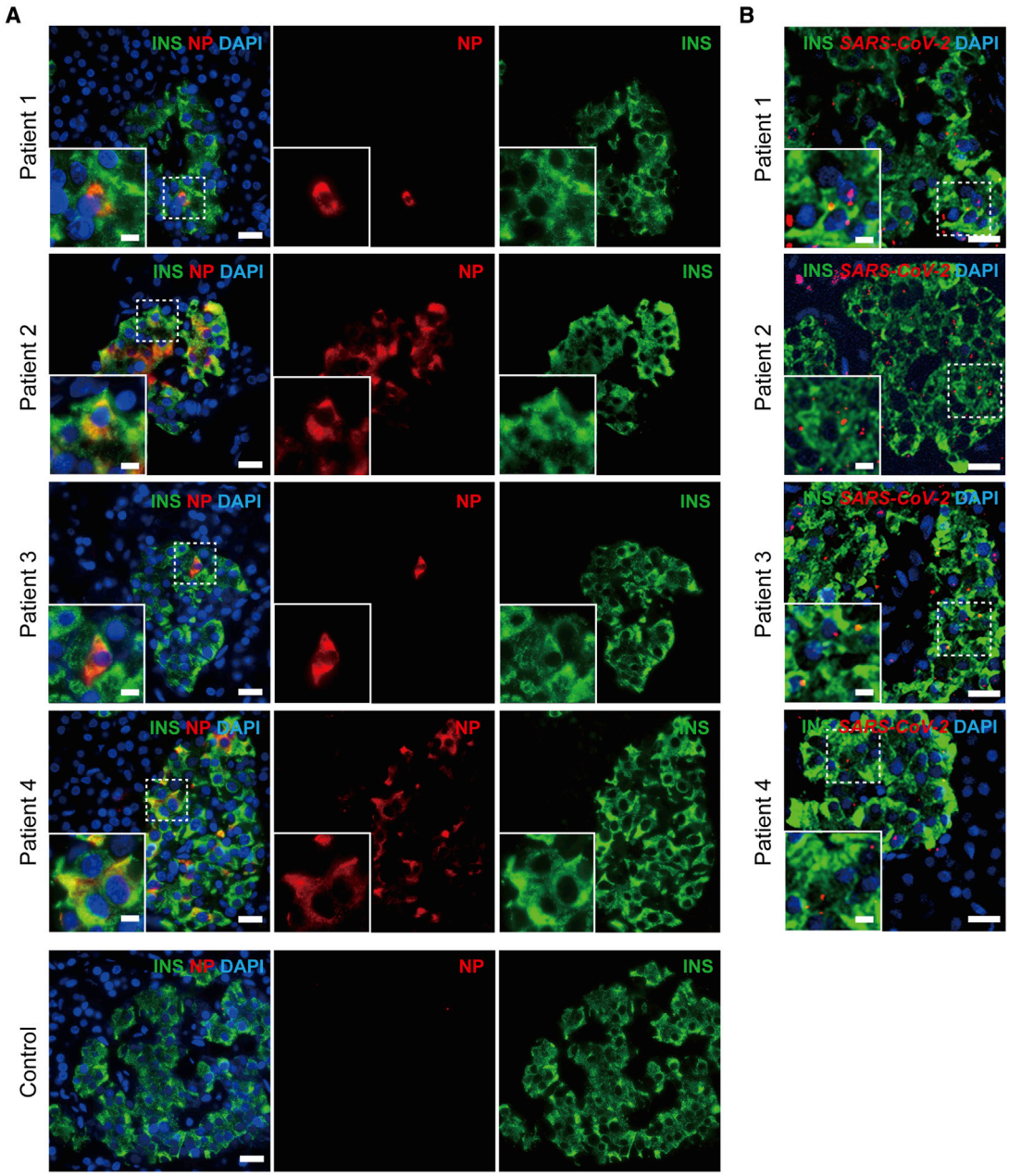

Figure 3. SARS-CoV-2 infects pancreatic β cells of patients with COVID-19

(A) Representative double immunofluorescence staining of pancreatic islets from patients with COVID-19 and healthy controls using antibodies against SARS-CoV-2 NP and INS.

(B) Representative multiplexed images of *in situ* hybridization against the SARS-CoV-2 spike mRNA, in combination with immunofluorescence staining of insulin (INS). SARS-CoV-2 spike mRNA expression (red dots) was detected within pancreatic β cells. The nuclei were stained using DAPI (blue) as a counterstain. Scale bars, 5 μm (A and B) and 2 μm (insets). See also Figure S3 and Table 3.

that SARS-CoV-2 infects β cells by staining pancreatic tissue sections from COVID-19 autopsies, the authors did not find β cells to be selectively infected by the SARS-CoV-2, but rather a large number of endocrine cells were infected in isolated islets. In contrast, we found that β cells are more susceptible to SARS-CoV-2 infection. Finally, the authors measured apoptosis via cleaved caspase-3 staining at 3 dpi and found no increased apoptosis in infected islets at 3 dpi. Our results indicate a significant increase in apoptotic β cells in infected islets at 2 and 6 dpi (Figure 4). This is further confirmed through phosphoproteomic analysis and subsequent identification of the specific upregulated kinases involved in apoptotic processes in isolated pancreatic islet post-SARS-CoV-2 SP treatment or virus infection (Figures S4 and S5).

There are a number of variations between our studies, one of which is the source of the SARS-CoV-2 used. Although we

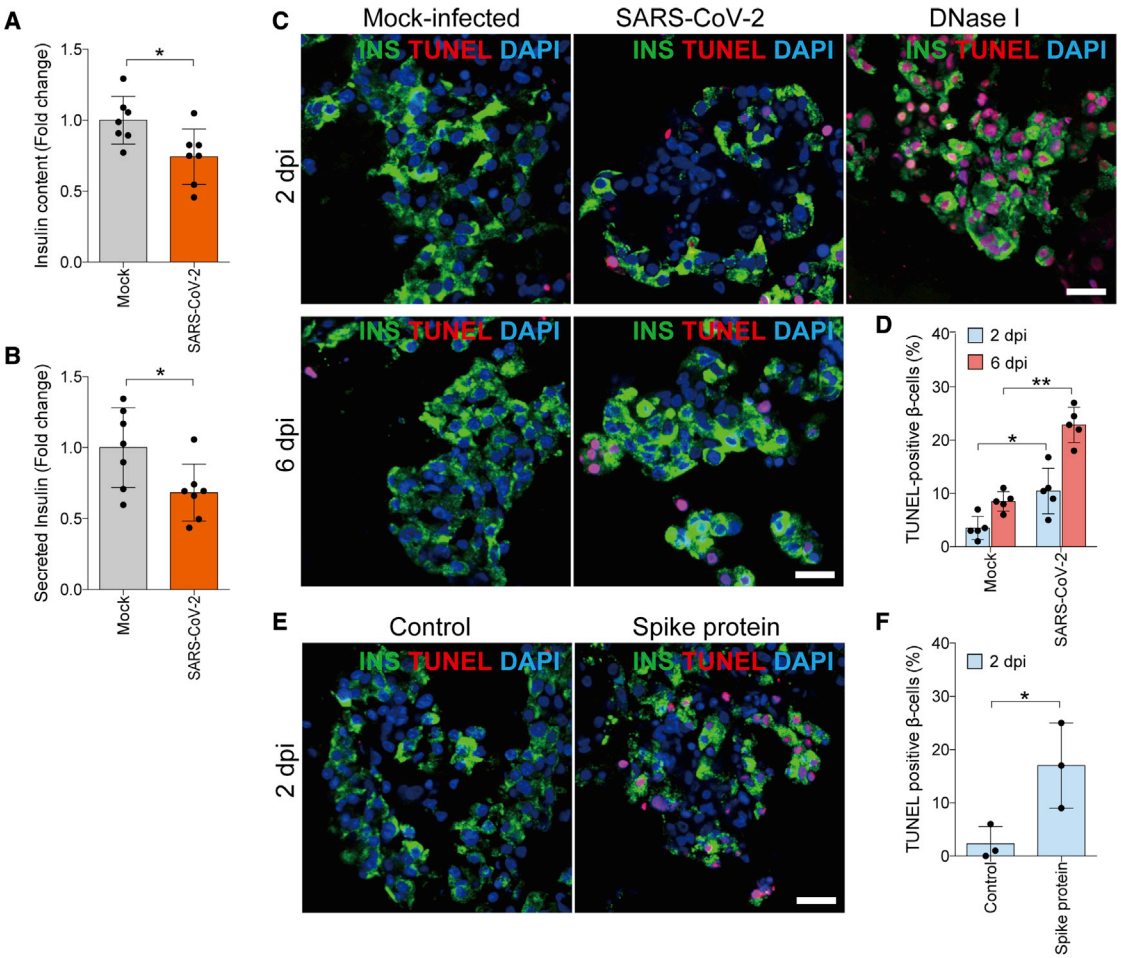

Figure 4. SARS-CoV-2 infection interferes with insulin content/secretion and induces β cell apoptosis

(A–F) Pancreatic islet functionality was analyzed by insulin content, glucose-stimulated insulin secretion (GSIS), and TUNEL staining *ex vivo*.

(A) Insulin content is decreased in SARS-CoV-2-infected islets compared with mock-treated islets.

(B) GSIS is decreased in SARS-CoV-2-infected islets compared with mock-treated islets.

(A and B) Error bars represent mean ± SD (data were collected from 7 healthy isolated human islets, donors 2–8; see Table 2). *$p < 0.05$, two-tailed Student's t test.

(C) Representative staining of β cell apoptosis by *in situ* TUNEL and DAPI staining in β cells (INS) of mock- or SARS-CoV-2-treated human islets. DNase-treated sections were used as a positive control in the TUNEL assay.

(D and F) Quantification of the percentages of islets containing TUNEL-positive β cells. Error bars represent mean ± SD (~500–1,000 cells were quantified from each of 3–5 separate healthy isolated human islets, donors 1–5 [D] and 7–9 [F]; see Table 2).

(E) Representative staining of β cell apoptosis by *in situ* TUNEL and DAPI staining in β cells (INS) of mock-treated versus SARS-CoV-2-SP-treated human islets. *$p < 0.05$, **$p < 0.01$, two-tailed Student's t test. Scale bars, 5 μm (C and E). See also Figures S3–S5 and Tables 2, S1, S2, and S3.

used the same SARS-CoV-2 D614G variant, the source is quite different. The clinically isolated virus used by Müller et al. originated from the Amsterdam University, Netherlands (010V-03903), while the clinical virus strain used in this paper was from UCSF, United States (CA-UCSF-0001C). Further studies are required to determine whether these different virus strains may affect pathological outcomes. In addition, our source of human islets is different. Our human islets are from patients of United States origin and may reflect different ethnicities. Given the scale of the ongoing epidemic, our findings emphasize the urgent need for the development of therapies to prevent COVID-19-induced diabetes, here informed through a combination of *ex vivo* tissue culture models, retrospective autopsy samples, and unbiased phosphoproteomic analysis.

Limitations of study

There are expected limitations to this study. First, the localization and quantification of pancreatic ACE2, TMPRSS2, NRP1, and TFRC are largely based on *ex vivo* and *in situ* analyses of protein (IHC and IF) expression in pancreatic tissues from a limited cohort of healthy or COVID-19 subjects. The histological analysis of these pancreatic tissue sections can only provide approximate predictions for ACE2, TMPRSS2, NRP1, and TFRC protein expression in isolated islets and islet cells and a general signature for their susceptibility to *in vitro* SARS-CoV-2 infection. This limitation is improved by our ability to infect human islet *ex vivo* and reconstitute several critical aspects of viral infection and pathogenesis, increasing our confidence in the results. For this study, we could not directly translate our *ex vivo*

observations of the dramatic decrease in insulin content and GSIS in SARS-CoV-2-infected human islets to the COVID-19 clinical samples in this study, as the insulin and blood glucose levels of these patients were not measured. Additional studies correlating patient serum markers of islet secretion of insulin, glucose levels, and COVID-19 status would be of considerable benefit to better understand virus effects on patients with typical versus severe COVID-19 disease.

Finally, phosphoproteomics was performed across the entire population of islet cell types, since single-cell phosphoproteomics is currently technically challenging. Therefore, we are unable to deconvolute any diversity of signaling pathways caused by the treatment of SARS-CoV-2 SP or SARS-CoV-2 infection in individual cell types in this study. Given the measured selectivity of infection in β cells and preponderance of β cells, we can reasonably estimate that the strong effects we observe reflect β cell alterations, rather than bystander effects.

STAR★METHODS

Detailed methods are provided in the online version of this paper and include the following:

- KEY RESOURCES TABLE
- RESOURCE AVAILABILITY
  - Lead contact
  - Materials Availability
  - Data and Code Availability
- EXPERIMENTAL MODEL AND SUBJECT DETAILS
  - Human pancreas tissue collection
- METHOD DETAILS
  - Virus production, islet infection, and drug treatment
  - Immunofluorescence immunohistochemistry (IF IHC) of cryosections
  - Immunofluorescence immunohistochemistry (IF IHC) of FFPE sections
  - SARS-COV-2 PCR
  - Antibodies and reagents
  - *In situ* hybridization staining
  - Microscopy
  - *In vitro* insulin secretion assays
  - TUNEL staining
  - Phosphopeptide Shotgun Proteomics
  - Kinase Set Enrichment Analysis (KSEA Analysis)
- QUANTIFICATION AND STATISTICAL ANALYSIS

SUPPLEMENTAL INFORMATION

Supplemental information can be found online at https://doi.org/10.1016/j.cmet.2021.05.013.

ACKNOWLEDGMENTS

The authors acknowledge members of the Kim laboratory, especially Jonathan Lam and Dr. Sangbin Park, for helpful discussions and assistance with islet experiments. We thank the Stanford Diabetes Research Center/Stanford Islet Research Core (supported by # P30DK116074). We thank the Stanford Diabetes Research Center/Stanford Islet Research Core (SDRC/SIRC), Alberta Diabetes Institute Islet (ADI) Research Core, IIDP, NDRI, and IIAM for islet and/or pancreas procurement, and especially the organ donors and their families. This work was supported by the National Institutes of Health R01DK127665 (P.K.J.), R01HD085901 (P.K.J.), R01GM121565 (P.K.J.), P30DK116074 (P.K.J.), R01AI149672-01 (G.P.N.), and U54-CA209971 (G.P.N.); Stanford Diabetes Research Center (SDRC) Pilot and Feasibility Research grant (P.K.J.); the Fast Grant Funding for COVID-19 Science (P.K.J. and G.P.N.); the Botnar Research Centre for Child Health Emergency Response to COVID-19 grant (S.J., M.S.M., G.P.N., and A.T.); a Bill and Melinda Gates Foundation COVID-19 Pilot Award (S.J. and G.P.N.); the Rachford & Carlotta A. Harris Endowed Chair (G.P.N.); California Institute for Regenerative Medicine (DISC2-09637) (J.V.N.); Defense Advanced Research Project Agency (HR001118S0037-PREPARE-FP-001) (J.V.N.); the Operndorf Foundation (J.V.N.); Stanford Respond. Innovate. Scale. Empower (RISE) COVID-19 crisis response trainee seed grant (C.-T.W., R.C., I.T.L., S.J., and T.N.); Stanford Translational Research and Applied Medicine (TRAM) pilot grant (I.T.L.); Thrasher Research Fund Early Career Award (I.T.L.); Stanford Maternal and Child Health Research Institute (MCHRI) Clinical (MD) Trainee Support Award (I.T.L., Ernest and Amelia Gallo endowed postdoctoral fellow); Leukemia & Lymphoma Society Career Development Program (S.J.); Cellular and Molecular Biology Training grant (NIH 5 T32 GM007276) (R.C.); and the Swiss National Science Foundation (SNSF; grant no. 320030_189275) (M.S.M.).

AUTHOR CONTRIBUTIONS

C.-T.W. conceived and coordinated the study. C.-T.W., P.V.L., Y.X., I.T.L., R.C., S.J., and T.N. designed and performed the experiments. C.-T.W., I.T.L., and T.N. performed the microscopy imaging. P.V.L. and Y.X. made virus and infected isolated human pancreatic islets. I.T.L., S.J., A.K.S., A.T., and M.S.M. obtained patient consent, and collected, processed, banked, and/or evaluated the human samples. R.C. and J.D. performed phosphopeptide shotgun proteomics. C.-T.W., I.T.L., R.C., J.D., T.N., and S.J. analyzed the data. C.-T.W., T.N., and S.J. conducted statistical analyses. R.J.B., R.L.W., and C.A.C. provided isolated pancreatic islets. B.Z. and H.C. assisted in experiments. Y.G. contributed novel tools that enabled the analysis. C.-T.W. and T.N. prepared the final figures. C.-T.W., I.T.L., S.J., and R.C. wrote the manuscript with contributions by P.V.L., J.V.N., A.T., M.S.M., and P.K.J. The co-first authors, C.-T.W., P.V.L., Y.X., I.T.L., R.C., S.J., and T.N. contributed equally and have the right to list their name first in their CV. Funding and supervision were provided by P.K.J. All authors reviewed and agreed with the content of this manuscript.

DECLARATION OF INTERESTS

The authors declare no competing interests.

Received: December 15, 2020
Revised: April 1, 2021
Accepted: May 7, 2021
Published: May 18, 2021

REFERENCES

Arda, H.E., Li, L., Tsai, J., Torre, E.A., Rosli, Y., Peiris, H., Spitale, R.C., Dai, C., Gu, X., Qu, K., et al. (2016). Age-dependent pancreatic gene regulation reveals mechanisms governing human beta cell function. Cell Metab. *23*, 909–920.

Baron, M., Veres, A., Wolock, S.L., Faust, A.L., Gaujoux, R., Vetere, A., Ryu, J.H., Wagner, B.K., Shen-Orr, S.S., Klein, A.M., et al. (2016). A single-cell transcriptomic map of the human and mouse pancreas reveals inter- and intra-cell population structure. Cell Syst. *3*, 346–360.e4.

Blodgett, D.M., Nowosielska, A., Afik, S., Pechhold, S., Cura, A.J., Kennedy, N.J., Kim, S., Kucukural, A., Davis, R.J., Kent, S.C., et al. (2015). Novel observations from next-generation RNA sequencing of highly purified human adult and fetal islet cell subsets. Diabetes *64*, 3172–3181.

Boddu, S.K., Aurangabadkar, G., and Kuchay, M.S. (2020). New onset diabetes, type 1 diabetes and COVID-19. Diabetes Metab. Syndr. *14*, 2211–2217.

Cantuti-Castelvetri, L., Ojha, R., Pedro, L.D., Djannatian, M., Franz, J., Kuivanen, S., van der Meer, F., Kallio, K., Kaya, T., Anastasina, M., et al. (2020). Neuropilin-1 facilitates SARS-CoV-2 cell entry and infectivity. Science *370*, 856–860.

Chee, Y.J., Ng, S.J.H., and Yeoh, E. (2020). Diabetic ketoacidosis precipitated by Covid-19 in a patient with newly diagnosed diabetes mellitus. Diabetes Res. Clin. Pract. *164*, 108166.

Chow, K.Y., Yeung, Y.S., Hon, C.C., Zeng, F., Law, K.M., and Leung, F.C. (2005). Adenovirus-mediated expression of the C-terminal domain of SARS-CoV spike protein is sufficient to induce apoptosis in Vero E6 cells. FEBS Lett. *579*, 6699–6704.

Clausen, T.M., Sandoval, D.R., Spliid, C.B., Pihl, J., Perrett, H.R., Painter, C.D., Narayanan, A., Majowicz, S.A., Kwong, E.M., McVicar, R.N., et al. (2020). SARS-CoV-2 infection depends on cellular heparan sulfate and ACE2. Cell *183*, 1043–1057.e15.

Coate, K.C., Cha, J., Shrestha, S., Wang, W., Gonçalves, L.M., Almaça, J., Kapp, M.E., Fasolino, M., Morgan, A., Dai, C., et al. (2020). SARS-CoV-2 cell entry factors ACE2 and TMPRSS2 are expressed in the microvasculature and ducts of human pancreas but are not enriched in beta cells. Cell Metab. *32*, 1028–1040.e4.

Daly, J.L., Simonetti, B., Klein, K., Chen, K.E., Williamson, M.K., Antón-Plágaro, C., Shoemark, D.K., Simón-Gracia, L., Bauer, M., Hollandi, R., et al. (2020). Neuropilin-1 is a host factor for SARS-CoV-2 infection. Science *370*, 861–865.

Dhanasekaran, D.N., and Reddy, E.P. (2008). JNK signaling in apoptosis. Oncogene *27*, 6245–6251.

Diemer, C., Schneider, M., Seebach, J., Quaas, J., Frösner, G., Schätzl, H.M., and Gilch, S. (2008). Cell type-specific cleavage of nucleocapsid protein by effector caspases during SARS coronavirus infection. J. Mol. Biol. *376*, 23–34.

Drake, J.M., Graham, N.A., Stoyanova, T., Sedghi, A., Goldstein, A.S., Cai, H., Smith, D.A., Zhang, H., Komisopoulou, E., Huang, J., et al. (2012). Oncogene-specific activation of tyrosine kinase networks during prostate cancer progression. Proc. Natl. Acad. Sci. USA *109*, 1643–1648.

Ebekozien, O.A., Noor, N., Gallagher, M.P., and Alonso, G.T. (2020). Type 1 diabetes and COVID-19: preliminary findings from a multicenter surveillance study in the U.S. Diabetes Care *43*, e83–e85.

Fang, L., Karakiulakis, G., and Roth, M. (2020). Are patients with hypertension and diabetes mellitus at increased risk for COVID-19 infection? Lancet Respir. Med. *8*, e21.

Fignani, D., Licata, G., Brusco, N., Nigi, L., Grieco, G.E., Marselli, L., Overbergh, L., Gysemans, C., Colli, M.L., Marchetti, P., et al. (2020). SARS-CoV-2 receptor angiotensin I-converting enzyme type 2 (ACE2) is expressed in human pancreatic β-cells and in the human pancreas microvasculature. Front. Endocrinol. (Lausanne) *11*, 596898.

Giacomelli, A., Pezzati, L., Conti, F., Bernacchia, D., Siano, M., Oreni, L., Rusconi, S., Gervasoni, C., Ridolfo, A.L., Rizzardini, G., et al. (2020). Self-reported olfactory and taste disorders in patients with severe acute respiratory coronavirus 2 infection: a cross-sectional study. Clin. Infect. Dis. *71*, 889–890.

Guo, B., Zhang, W., Xu, S., Lou, J., Wang, S., and Men, X. (2016). GSK-3β mediates dexamethasone-induced pancreatic beta cell apoptosis. Life Sci. *144*, 1–7.

Haberger, V., Elgner, F., Roos, J., Bender, D., and Hildt, E. (2020). Regulation of the transferrin receptor recycling in hepatitis C virus-replicating cells. Front. Cell Dev. Biol. *8*, 44.

Hernandez-Armenta, C., Ochoa, D., Gonçalves, E., Saez-Rodriguez, J., and Beltrao, P. (2017). Benchmarking substrate-based kinase activity inference using phosphoproteomic data. Bioinformatics *33*, 1845–1851.

Hoffmann, M., Kleine-Weber, H., Schroeder, S., Krüger, N., Herrler, T., Erichsen, S., Schiergens, T.S., Herrler, G., Wu, N.-H., Nitsche, A., et al. (2020). SARS-CoV-2 cell entry depends on ACE2 and TMPRSS2 and is blocked by a clinically proven protease inhibitor. Cell *181*, 271–280.e8.

Hollstein, T., Schulte, D.M., Schulz, J., Glück, A., Ziegler, A.G., Bonifacio, E., Wendorff, M., Franke, A., Schreiber, S., Bornstein, S.R., and Laudes, M. (2020). Autoantibody-negative insulin-dependent diabetes mellitus after SARS-CoV-2 infection: a case report. Nat. Metab. *2*, 1021–1024.

Hornbeck, P.V., Zhang, B., Murray, B., Kornhauser, J.M., Latham, V., and Skrzypek, E. (2015). PhosphoSitePlus, 2014: mutations, PTMs and recalibrations. Nucleic Acids Res. *43*, D512–D520.

Kim, S., Whitener, R.L., Peiris, H., Gu, X., Chang, C.A., Lam, J.Y., Camunas-Soler, J., Park, I., Bevacqua, R.J., Tellez, K., et al. (2020). Molecular and genetic regulation of pig pancreatic islet cell development. Development *147*, dev186213.

Kusmartseva, I., Wu, W., Syed, F., Van Der Heide, V., Jorgensen, M., Joseph, P., Tang, X., Candelario-Jalil, E., Yang, C., Nick, H., et al. (2020). Expression of SARS-CoV-2 entry factors in the pancreas of normal organ donors and individuals with COVID-19. Cell Metab. *32*, 1041–1051.e6.

Lamers, M.M., Beumer, J., van der Vaart, J., Knoops, K., Puschhof, J., Breugem, T.I., Ravelli, R.B.G., Paul van Schayck, J., Mykytyn, A.Z., Duimel, H.Q., et al. (2020). SARS-CoV-2 productively infects human gut enterocytes. Science *369*, 50–54.

Lee, I.T., Nakayama, T., Wu, C.T., Goltsev, Y., Jiang, S., Gall, P.A., Liao, C.K., Shih, L.C., Schürch, C.M., McIlwain, D.R., et al. (2020). ACE2 localizes to the respiratory cilia and is not increased by ACE inhibitors or ARBs. Nat. Commun. *11*, 5453.

Li, Y., Renner, D.M., Comar, C.E., Whelan, J.N., Reyes, H.M., Cardenas-Diaz, F.L., Truitt, R., Tan, L.H., Dong, B., Alysandratos, K.D., et al. (2020). SARS-CoV-2 induces double-stranded RNA-mediated innate immune responses in respiratory epithelial derived cells and cardiomyocytes. bioRxiv. https://doi.org/10.1101/2020.09.24.312553.

Linding, R., Jensen, L.J., Pasculescu, A., Olhovsky, M., Colwill, K., Bork, P., Yaffe, M.B., and Pawson, T. (2008). NetworKIN: a resource for exploring cellular phosphorylation networks. Nucleic Acids Res. *36*, D695–D699.

Manser, E., Leung, T., Salihuddin, H., Zhao, Z.S., and Lim, L. (1994). A brain serine/threonine protein kinase activated by Cdc42 and Rac1. Nature *367*, 40–46.

Meier, F., Brunner, A.D., Koch, S., Koch, H., Lubeck, M., Krause, M., Goedecke, N., Decker, J., Kosinski, T., Park, M.A., et al. (2018). Online parallel accumulation-serial fragmentation (PASEF) with a novel trapped ion mobility mass spectrometer. Mol. Cell. Proteomics *17*, 2534–2545.

Menter, T., Haslbauer, J.D., Nienhold, R., Savic, S., Hopfer, H., Deigendesch, N., Frank, S., Turek, D., Willi, N., Pargger, H., et al. (2020). Postmortem examination of COVID-19 patients reveals diffuse alveolar damage with severe capillary congestion and variegated findings in lungs and other organs suggesting vascular dysfunction. Histopathology *77*, 198–209.

Müller, J.A., Groß, R., Conzelmann, C., Krüger, J., Merle, U., Steinhart, J., Weil, T., Koepke, L., Bozzo, C.P., Read, C., et al. (2021). SARS-CoV-2 infects and replicates in cells of the human endocrine and exocrine pancreas. Nat. Metab. *3*, 149–165.

Naguib, M.N., Raymond, J.K., and Vidmar, A.P. (2021). New onset diabetes with diabetic ketoacidosis in a child with multisystem inflammatory syndrome due to COVID-19. J. Pediatr. Endocrinol. Metab. *34*, 147–150.

Ochoa, D., Jonikas, M., Lawrence, R.T., El Debs, B., Selkrig, J., Typas, A., Villén, J., Santos, S.D., and Beltrao, P. (2016). An atlas of human kinase regulation. Mol. Syst. Biol. *12*, 888.

Puelles, V.G., Lütgehetmann, M., Lindenmeyer, M.T., Sperhake, J.P., Wong, M.N., Allweiss, L., Chilla, S., Heinemann, A., Wanner, N., Liu, S., et al. (2020). Multiorgan and renal tropism of SARS-CoV-2. N. Engl. J. Med. *383*, 590–592.

Rubino, F., Amiel, S.A., Zimmet, P., Alberti, G., Bornstein, S., Eckel, R.H., Mingrone, G., Boehm, B., Cooper, M.E., Chai, Z., et al. (2020). New-onset diabetes in Covid-19. N. Engl. J. Med. *383*, 789–790.

Segerstolpe, Å., Palasantza, A., Eliasson, P., Andersson, E.-M., Andréasson, A.C., Sun, X., Picelli, S., Sabirsh, A., Clausen, M., Bjursell, M.K., et al. (2016). Single-cell transcriptome profiling of human pancreatic islets in health and type 2 diabetes. Cell Metab. *24*, 593–607.

Simeonovic, C.J., Popp, S.K., Starrs, L.M., Brown, D.J., Ziolkowski, A.F., Ludwig, B., Bornstein, S.R., Wilson, J.D., Pugliese, A., Kay, T.W.H., et al. (2018). Loss of intra-islet heparan sulfate is a highly sensitive marker of type 1 diabetes progression in humans. PLoS One *13*, e0191360.

Singh, A.K., and Singh, R. (2020). Hyperglycemia without diabetes and new-onset diabetes are both associated with poorer outcomes in COVID-19. Diabetes Res. Clin. Pract. *167*, 108382.

Suárez-Fariñas, M., Tokuyama, M., Wei, G., Huang, R., Livanos, A., Jha, D., Levescot, A., Irizar, H., Kosoy, R., Cording, S., et al. (2021). Intestinal inflammation modulates the expression of ACE2 and TMPRSS2 and potentially overlaps with the pathogenesis of SARS-CoV-2-related disease. Gastroenterology *160*, 287–301.e20.

Subramanian, A., Tamayo, P., Mootha, V.K., Mukherjee, S., Ebert, B.L., Gillette, M.A., Paulovich, A., Pomeroy, S.L., Golub, T.R., Lander, E.S., and Mesirov, J.P. (2005). Gene set enrichment analysis: a knowledge-based approach for interpreting genome-wide expression profiles. Proc. Natl. Acad. Sci. USA *102*, 15545–15550.

Tang, X., Yang, M., Duan, Z., Liao, Z., Liu, L., Cheng, R., Fang, M., Wang, G., Liu, H., Xu, J., et al. (2020). Transferrin receptor is another receptor for SARS-CoV-2 entry. bioRxiv. https://doi.org/10.1101/2020.10.23.350348.

Tournier, C., Hess, P., Yang, D.D., Xu, J., Turner, T.K., Nimnual, A., Bar-Sagi, D., Jones, S.N., Flavell, R.A., and Davis, R.J. (2000). Requirement of JNK for stress-induced activation of the cytochrome c-mediated death pathway. Science *288*, 870–874.

Unsworth, R., Wallace, S., Oliver, N.S., Yeung, S., Kshirsagar, A., Naidu, H., Kwong, R.M.W., Kumar, P., and Logan, K.M. (2020). New-onset type 1 diabetes in children during COVID-19: multicenter regional findings in the U.K. Diabetes Care *43*, e170–e171.

Wada, T., and Penninger, J.M. (2004). Mitogen-activated protein kinases in apoptosis regulation. Oncogene *23*, 2838–2849.

Yang, X., Yu, Y., Xu, J., Shu, H., Xia, J., Liu, H., Wu, Y., Zhang, L., Yu, Z., Fang, M., et al. (2020). Clinical course and outcomes of critically ill patients with SARS-CoV-2 pneumonia in Wuhan, China: a single-centered, retrospective, observational study. Lancet Respir. Med. *8*, 475–481.

Yu, G., Wang, L.G., Han, Y., and He, Q.Y. (2012). clusterProfiler: an R package for comparing biological themes among gene clusters. Omics *16*, 284–287.

Zheng, Y.Y., Ma, Y.T., Zhang, J.Y., and Xie, X. (2020). COVID-19 and the cardiovascular system. Nat. Rev. Cardiol. *17*, 259–260.

Zhu, N., Wang, W., Liu, Z., Liang, C., Wang, W., Ye, F., Huang, B., Zhao, L., Wang, H., Zhou, W., et al. (2020a). Morphogenesis and cytopathic effect of SARS-CoV-2 infection in human airway epithelial cells. Nat. Commun. *11*, 3910.

Zhu, N., Zhang, D., Wang, W., Li, X., Yang, B., Song, J., Zhao, X., Huang, B., Shi, W., Lu, R., et al. (2020b). A novel coronavirus from patients with pneumonia in China, 2019. N. Engl. J. Med. *382*, 727–733.

Ziolkowski, A.F., Popp, S.K., Freeman, C., Parish, C.R., and Simeonovic, C.J. (2012). Heparan sulfate and heparanase play key roles in mouse beta cell survival and autoimmune diabetes. J. Clin. Invest. *122*, 132–141.

STAR★METHODS

KEY RESOURCES TABLE

REAGENT or RESOURCE	SOURCE	IDENTIFIER
Antibodies		
Rabbit anti-SARS-CoV-2-NP	GeneTex	Cat# GTX135361; RRID: AB_2887484
Mouse anti-SARS-CoV-2-NP	Thermo Fisher	Cat# MA1-7403; RRID: AB_1018420
Mouse anti-SARS-CoV-2-SP	GeneTex	Cat# GTX632604; RRID: AB_2864418
Rabbit anti-ACE2	Abcam	Cat# ab15348; RRID: AB_301861
Mouse anti-TMPRSS2	Millipore	Cat# MABF2158
Mouse anti-NRP1	Santa Cruz	Cat# sc-5307; RRID: AB_2282634
Rabbit anti-NRP1	Abcam	Cat# ab81321; RRID: AB_1640739
Rabbit anti-NRP1	Atlas	Cat# HPA030278; RRID: AB_10601976
Mouse anti-TFRC	Thermo Fisher	Cat# 13-6800; RRID: AB_2533029
Rabbit anti-TFRC	Atlas	Cat# HPA028598; RRID: AB_10601599
Mouse anti-Insulin	Cell Signaling	Cat# 8138S; RRID: AB_10949314
Mouse anti-Insulin	Santa Cruz	Cat# sc-8033; RRID: AB_627285
Rabbit anti-glucagon	ProteinTech	Cat# 15954-1-AP; RRID: AB_2878200
Mouse anti-glucagon	Abcam	Cat# ab10988; RRID: AB_297642
Mouse-somatostatin	Santa Cruz	Cat# sc-55565; RRID: AB_831726
Mouse-somatostatin	Santa Cruz	Cat# sc-74556; RRID: AB_2271061
Mouse anti-CD31	BD	Cat# 550389; RRID: AB_2252087
Mouse anti-CD31	Novus	Cat# NBP2-47785; RRID: AB_2864381
Rabbit anti- Phospho-JNK1/2	Cell Signaling	Cat# 4668T
Rabbit anti- Phospho-PAK1/2	Cell Signaling	Cat# 2601S; RRID: AB_330220
Bacterial and virus strains		
SARS-CoV-2	Joe DeRisi Lab, UCSF	SARS-CoV-2/human/USA/CA-UCSF-0001C/2020
Biological samples		
Human pancreatic islets	Integrated Islet Distribution Program (IIDP)	Table 2
Chemicals, peptides, and recombinant proteins		
DMSO	Sigma-Aldrich	Cat# 276855
EG00229	Sigma-Aldrich	Cat# SML1367
DAPI	Bio Trend	Cat# 40043
Pen/Strep	Thermo Fisher	Cat# 15140163
Paraformaldehyde	AlfaAesar	Cat# 433689M
Normal Donkey Serum	Jackson ImmunoResearch	Cat# 017-000-121
NP40	Sigma	Cat# 11332473001
The unrelated mock peptide: KKHKNQRSRKKHKNQRSR	Genscript	N/A
The NRP1 peptide for blocking assay	Abcam	Cat# ab189308
The TFRC peptide for blocking assay: DQARSAFSNLFGGEPLSYTRFSLARQ	GenScript	N/A
The SARS-CoV-2 NP peptide for blocking assay: STGSNQNGERSGARSK	GenScript	N/A
BSA	Sigma	Cat# A6003-25G
1X PBS	Corning	Cat# 46-013-CM
Triton X-100	USB	Cat# 22686
OCT compound	VWR	Cat# 25608-930

(*Continued on next page*)

Continued

REAGENT or RESOURCE	SOURCE	IDENTIFIER
Saponin	Sigma-Aldrich	Cat# S7900
Fluoromount-G	SouthernBiotech	Cat# 0100-01
Dako Target Retrieval Solution, pH 9	DAKO Agilent	Cat# S236784-2
ProLong Gold Antifade mounting medium with DAPI	Thermo Fisher	Cat# P36931
Hoechst	Thermo Fisher	Cat# 33342
GlutaMax	life	Cat# 35050-079
Critical commercial assays		
Human insulin ELISA kit	Mercodia	Cat# 10-1113-01
In Situ Cell Death Detection Kit, TMR red	Sigma-Aldrich	Cat# 12156792910
TaqMan 2019-nCoV Control Kit v1	Thermo Fisher	Cat# A47533
RNAscope Multiplex Fluorescent Reagent Kit v2	Bio-Techne	Cat# 323100
TSA Cyanine 3	Akoya Biosciences	Cat# NEL744001KT
High-Select Fe-NTA Phosphopeptide Enrichment Kit	Thermo Scientific	Cat# A32992
Deposited data		
RNA-seq data for FACS purified human alpha and beta cells (Blodgett et al., 2015)	NCBI Gene Expression Omnibus	GEO: GSE67543
RNA-seq data for FACS purified human alpha and beta cells (Arda et al., 2016)	NCBI Gene Expression Omnibus	GEO: GSE57973
RNA-seq data for FACS purified human alpha, beta, and delta cells (Kim et al., 2020)	NCBI Gene Expression Omnibus	GEO: GSE143889
Phosphoproteomics data of SARS-CoV-2 infected and Spike protein treated human pancreatic islets	This paper	PRIDE: PXD025629
Oligonucleotides		
SARS-CoV-2 spike mRNA	Bio-Techne	Cat# 848561
Software and algorithms		
ImageJ	NIH	https://imagej.nih.gov/ij/
Zen black	Carl Zeiss	https://www.zeiss.com/microscopy/us/products/microscope-software/zen.html

RESOURCE AVAILABILITY

Lead contact

Further information and requests for resources and reagents should be directed to and will be fulfilled by the Lead Contact, Peter Jackson (pjackson@stanford.edu).

Materials Availability

This study did not generate new unique reagents.

Data and Code Availability

The analysis code used to support the findings of this study are available at https://github.com/bmyury/membrane_ACE2_quantitation.

EXPERIMENTAL MODEL AND SUBJECT DETAILS

Human pancreas tissue collection

De-identified human pancreatic islets were obtained from adult organ donors without a history of diabetes or glucose intolerance. Islets were procured through the Integrated Islet Distribution Program, Alberta Diabetes Institute IsletCore, and the International Institute for the Advancement of Medicine. SARS-CoV-2 infected pancreas tissue was obtained during autopsy and processed as

previously described (Menter et al., 2020); the procedure was approved by the ethics commission of Northern Switzerland (EKNZ; study ID: 2020-00969). All patients with COVID-19 or their relatives consented to the use of tissue for research purposes. The characteristics of the autopsy and islet donors are summarized in Tables 1, 2, and 3.

METHOD DETAILS

Virus production, islet infection, and drug treatment

A549 cells stably expressing *ACE2* under CMV promoter were infected with SARS-CoV-2 clinical isolate of the pandemic D614G variant (SARS-CoV-2/human/USA/CA-UCSF-0001C/2020, kindly provided by Sara Sunshine and Joe DeRisi) with MOI ~0.05 in MEM medium supplemented with 2% FBS and penicillin/streptavidin (Gibco). 3 days after infection, the medium was collected and cleared from cell debris by centrifugation at 3,000 g for 10 min at 4 C. The virus titers were measured by plaque assay. To infect the islets, 100 ul of virus suspension (5-10x10^6 PFU per ml) was added to 1 ml of the pancreatic islet culture and incubated at 37°C for the indicated time. Small molecules were dissolved in DMSO (276855, Sigma-Aldrich). Islets were first treated with 100 μM EG00229 (SML1367, Sigma-Aldrich) or DMSO for 1 hour before infection with SARS-CoV-2. Islets were fixed at 2 dpi.

Immunofluorescence immunohistochemistry (IF IHC) of cryosections

For cryosections, isolated human islets were fixed in 4% paraformaldehyde in 1X PBS for 1 h, embedded in collagen I (Becton-Dickinson, San Jose, CA, USA) 4% (wt/vol.) and then fixed on ice in 4% paraformaldehyde in 1X PBS for another 20 min, followed by three 5 min washes with 1X PBS and equilibration in 30% sucrose/1X PBS overnight. Tissue specimens were processed for OCT-embedded, 6-μm cryosections.

Cryosections were blocked with 5% normal donkey serum (017-000-121, Jackson ImmunoResearch) in IF buffer (3% BSA and 0.4% saponin in PBS; for all else: 3% BSA and 0.1% NP-40 in PBS) at room temperature for 1 hour. Samples were incubated with primary antibody in IF buffer at room temperature for overnight at 4°C, followed by 5 washes with IF buffer. Samples were then incubated with fluorescent-labeled secondary antibody at room temperature for 1 hour, followed by a 5 min incubation with 4',6-dia-midino-2-phenylindole (DAPI) in PBS at room temperature for 5min and 3 washes with IF buffer. Coverslips were mounted with Fluoromount-G (0100-01, SouthernBiotech) onto glass slides followed by image acquisition.

Immunofluorescence immunohistochemistry (IF IHC) of FFPE sections

Sections were cut to 4 μm thickness onto frosted glass slides at the Stanford University Histology Service Center and University Hospital Basel. H&E-stained sections were obtained from each formalin-fixed paraffin-embedded (FFPE) block. Deparaffinization, rehydration, and heat-induced epitope retrieval (HIER) were performed on a ST4020 small linear stainer (Leica). For deparaffinization, slides were baked at 70 °C for 1 h, followed by rehydration in descending concentrations of ethanol (100% twice, 95% twice, 80%, 70%, ddH2O twice; each step for 3 min). Washes were performed using a Leica ST4020 Linear Stainer (Leica Biosystems, Wetzlar, Germany) programmed to three dips per wash for 30 s each. HIER was performed in a Lab VisionTM PT module (Thermo Fisher) using Dako Target Retrieval Solution, pH 9 (S236784-2, DAKO Agilent) at 97 °C for 10 min and cooled down to 65 °C. After further cooling to room temperature for 30 min, slides were washed for 5-10 min three times in Tris-Buffered Saline (TBS), containing 0.1% Tween 20 (Cell Marque; TBS-T). Sections were then blocked in 5% normal donkey serum ((D9663, Sigma-Aldrich) in TBS-T at room temperature for 1 h, followed by incubation with primary antibodies in the blocking solution. After one overnight incubation of primary antibodies in 4 °C, sections were washed three times with TBS-T and stained with the appropriate secondary antibodies in PBS with 3% bovine serum albumin, 0.4% saponin, and 0.02% sodium azide at room temperature for 1 h. Following this, sections were washed three times with TBS-T and mounted with ProLong Gold Antifade mounting medium with DAPI (Invitrogen). Hoechst (33342, Thermo) was also used in the second to last TBS-T wash for additional nuclear staining. For the peptide blocking assay, the NRP1 (Abcam, ab81321), TFRC (Thermo, # 13-6800), and SARS-CoV-2 NP (GeneTex, GTX135361) antibodies were preincubated with a 20-fold molar excess of the immunizing peptide or an unrelated mock peptide for 3 hours with rotation at room temperature immediately before primary antibody staining. The peptides used are described below.

SARS-COV-2 PCR

For detection of SARS-CoV-2, RNA was first isolated from formalin-fixed and paraffin embedded pancreas tissue by using the Maxwell RSC RNA FFPE Kit (Promega, Madison, WI, USA) according to the manufacturer's protocol. Afterwards, TaqMan reverse transcription polymerase chain reaction (RT-PCR) was performed by using the TaqMan 2019-nCoV Control Kit v1 (A47533, ThermoFisher Scientific) to target three different viral genomic regions (ORF1ab, S and N) and the human RPPH1 gene (RNAse-P). According to the manufacturer's protocol, a C_T value below 37 in at least two out of three viral genomic regions was considered positive. A case was considered negative if C_T values were above 40. Values between 37 and 40 were considered indeterminate and the assay was repeated. Samples were always run as duplicates.

Antibodies and reagents

Antibodies used include the following: rabbit anti-SARS-CoV-2-NP (GeneTex, GTX135361, 1:2,000), mouse anti-SARS-CoV-2-NP (Thermo Fisher, MA1-7403, 1:200), mouse anti-SARS-CoV-2-SP (GeneTex, GTX632604, 1:500), rabbit anti-ACE2 (Abcam, ab15348, 1:200), mouse anti-TMPRSS2 (Millipore, MABF2158, 1:200), mouse anti-NRP1 (Santa Cruz, sc-5307, 1:200), rabbit

anti-NRP1 (Abcam, ab81321, 1:200), rabbit anti-NRP1 (Atlas, HPA030278, 1:200), mouse anti-TFRC (Thermo Fisher, # 13-6800, 1:200), rabbit anti-TFRC (Atlas, HPA028598, 1:200), mouse anti-Insulin (Cell Signaling, 8138S, 1:4,000), mouse anti-Insulin (Santa Cruz, sc-8033, 1:1,000), rabbit anti-glucagon (ProteinTech, 15954-1-AP, 1:3,000), mouse anti-glucagon (Abcam, ab10988, 1:4,000), mouse-somatostatin (Santa Cruz, sc-55565, 1:6,000), mouse-somatostatin (Santa Cruz, sc-74556, 1:2,000), mouse anti-CD31 (BD, 550389, 1:100), mouse anti-CD31 (Novus, NBP2-47785, 1:200), rabbit anti- Phospho-JNK1/2 (Cell Signaling, 4668T, 1:100), and rabbit anti- Phospho-PAK1/2 (Cell Signaling, 2601S, 1:100). Spike protein (BPS Bioscience, 100688) was used in the apoptosis experiment in Figures 4E and 4F. The immunizing peptides for the peptide blocking assay were NRP1 (Abcam, ab189308), TFRC (custom synthesized through GenScript using sequences provided in confidence by Thermo Fisher), and SARS-CoV-2 NP (custom synthesized through GenScript using sequences provided in confidence by GeneTex). The sequence of the unrelated mock peptide used for the peptide blocking assay was KKHKNQRSRKKHKNQRSR (Genscript).

In situ hybridization staining

Rehydration and HIER of tissue sections were performed as described above and in Lee et al. (2020). After cooling to room temperature, slides were washed for 2 × 2 min ddH2O before a 15 min H2O2 block at 40 °C (322335, Bio-Techne). Slides were then washed for 2 × 2 min ddH2O before an overnight hybridization at 40 °C with probes against the SARS-CoV-2 spike mRNA (848561, Bio-Techne). Amplification of the ISH probes was performed the next day according to manufacturer's protocol (323100, Bio-Techne), with the final deposition of Cyanine 3 for SARS-CoV-2 spike mRNA probe targets (NEL744001KT, Akoya Biosciences). Slides were then processed as described above for IF IHC staining for mouse anti-insulin (Cell Signaling, 8138S, 1:4000).

Microscopy

Fluorescence-immunolabeled images were acquired using a Zeiss AxioImager Z1 microscope or a Marianas spinning disk confocal (SDC) microscopy (Intelligent Imaging Innovations). Post-imaging processing was performed using ZEN (Carl Zeiss). Final figures were organized using Adobe Illustrator.

In vitro insulin secretion assays

GSIS was performed 6 days post infection. Batches of 25 islets were used for in vitro secretion assays. Islets were incubated at a glucose concentration of 2.8 mM for 1 h as an initial equilibration period. Subsequently, islets were incubated at 2.8 mM glucose concentration for 1 h. Supernatant was taken and stored for insulin quantification. Islets were incubated at 16.7 mM glucose concentration for another 1 h. Supernatant was taken and stored for insulin quantification. Islets were then lysed in an acid-ethanol solution (1.5% HCL in 75% ethanol) to extract the total cellular insulin or glucagon content. Secreted human insulin in the supernatants and islet lysates were quantified using a human insulin ELISA kit (Mercodia). Secreted insulin levels were divided by total insulin content and presented as a percentage of total insulin content and normalized to values obtained at 2.8 mM glucose. All secretion assays were carried out in RPMI 1640 (Gibco) and the above-mentioned glucose concentrations.

TUNEL staining

Cellular apoptosis was measured by TUNEL staining according to the manufacturer's instructions (Roche, Berlin, Germany). The proportion of TUNEL-positive nuclei in pancreatic β cell was determined through image analysis of the cryosections. The number of TUNEL-positive cells in pancreatic islets was counted under an Everest deconvolution workstation (Intelligent Imaging Innovations) equipped with a Zeiss AxioImager Z1 microscope and a CoolSnapHQ cooled CCD camera (Roper Scientific).

Phosphopeptide Shotgun Proteomics

Isolated human islet cells were treated with SARS-CoV-2 spike protein for 15, 30 minutes or with vehicle (water) for 30 minutes. Cells were harvested, lysed, reduce, and alkylated using 100 μl of lysis buffer (6M Guanidine Hydrochloride, 100 mM Tris-HCl pH 8.0, 10 mM TCEP, 10 mM CAA) and boiled 60°C for 1 hour. Proteins were precipitated by adding 100 μl methanol, vortexed, 50 μl chloroform, vortexed, 100 μl water, vortexed, and centrifuged at 13,000g for 2 minutes. The top aqueous layer was removed, 200 μl of methanol was added, vortexed, and centrifuged at 13,000g for 3 minutes. Methanol was removed and dried proteins were resuspended using 200mM HEPES pH 8.5. Proteins were digested using Trypsin/Lys-C overnight at 37°C 250 RPM. Sample was acidified using TFA and cleaned using stage tips. Stage tips were created using 5 layers of C18 filters packed into a P200 tip. The stage tips were activated using methanol, equilibrated twice with equilibration buffer (5% ACN, 0.5% TFA). Sample were bound, washed twice with equilibration buffer, and eluted using elution buffer (50% ACN, 0.1% FA). Eluted samples were dried using a Speed-Vac and resuspended using Binding/Wash Buffer in High-Select Fe-NTA Phosphopeptide Enrichment Kit (Thermo Scientific, A32992). The peptides were enriched for phosphopeptides according to the manufacturer's instructions. Eluted samples were eluted and resuspended using Solution A (2% ACN, 0.1% FA).

Samples were analyzed using the timsTOF Pro (Bruker Daltonics) (Meier et al., 2018), an ion-mobility spectrometry quadrupole time of flight mass spectrometer. Specifically, a nanoElute (Bruker Daltonics) high pressure nanoflow system was connected to the timsTOF Pro. Peptides were delivered to a reversed phase analytical column (10 cm x 75 μm i.d., Bruker 1866154). Liquid chromatography was performed at 50 °C and peptides were separated on the analytical column using a 48 min gradient (solvent A: 2% ACN, 0.1% FA; solvent B: 0.1% FA, in ACN) at a flow rate of 500 nl/min. A linear gradient from 2-35 % B was applied for 45 min, followed by a step to 95% B for 1.5 min and 3 min of washing at 95% B. The timsTOF Pro was operated in PASEF mode with the following

settings: Mass Range 100 to 1700m/z, 1/K0 Start 0.85 V·s/cm2, End 1.3 V·s/cm2, Ramp time 100ms, Lock Duty Cycle to 100%, Capillary Voltage 1700, Dry Gas 3 l/min, Dry Temp 200°C, PASEF settings: 4 MS/MS, charge range 0-5, active exclusion for 0.04 min, Scheduling Target intensity 20000, Intensity threshold 500, CID collision energy 10eV.

For analysis, Bruker raw data files were processed using Byonic software (Protein Metrics) to identify peptides and proteins using the NCBI Homo sapiens refseq protein database. Data were searched with 20 ppm error tolerance for precursor and 40 ppm for fragment ions using QTOF/HCD fragmentation type. Besides standard variable modifications, we searched for S/T/Y phosphorylation and set 1 % FDR for protein identifications.

Kinase Set Enrichment Analysis (KSEA Analysis)

Counts for phosphosites between two technical replicates were summed after the total counts per sample were normalized to the median of total counts. The counts were then $\log_2$-transformed and quantile normalized. Batch correction was done using ComBat function from the sva package from Bioconductor and the $\log_2$-transformation was undone to obtain the counts for differential expression analysis. Differential expression analysis was conducted with the msms.glm.pois function from the msmsTests package from Bioconductor (Josep Gregori, Alex Sanchez and Josep Villanueva (2020). msmsTests: LC-MS/MS Differential Expression Tests. R package version 1.26.0.). KSEA was calculated with the ksea function from ksea package from GitHub (David Ochoa (2020). ksea: Kinase Activity Prediction based in Quantitative Phosphoproteomic Data. R package version 0.1.2.) using a kinase substrate database created from PhosphositePlus (Hornbeck et al., 2015) and NetworKin (Linding et al., 2008). p-values were adjusted using Benjamini-Hochberg procedure. GO ORA was conducted using enrichGO function from the clusterProfiler package from Bioconductor (Yu et al., 2012) and the database org.Hs.eg.db package from Bioconductor (Marc Carlson (2020). org.Hs.eg.db: Genome wide annotation for Human. R package version 3.11.4.).

QUANTIFICATION AND STATISTICAL ANALYSIS

For signal quantification, samples were stained simultaneously in batch with the primary antibodies (ex. ACE2, TMPRSS2, NRP1, TFRC, insulin, glucagon as described above) using the same master mixes and identical incubation times under similar staining conditions described above. Exposure times under confocal microscopy were identical for the quantified samples. Quantification was performed using a custom script developed in the FIJI package of ImageJ as previously described (Lee et al., 2020). Briefly, a binary mask was created by thresholding the insulin and glucagon channels using selected cutoff values to generate a comprehensive outline of each channel. Insulin- and glucagon-positive regions were segmented using continuity of high signal regions on a binary mask. Finally, the signals of proteins of interest within the segmented regions were computed. While the experimenters were not strictly blinded to the samples, all sample processing, staining, and data acquisition were performed in parallel under identical conditions without regard to the specific identity of the samples. Quantification used a custom script developed in the FIJI package of ImageJ as previously described (Lee et al., 2020). Experimental sample sizes were not predetermined given the exploratory nature of the work and the limited availability of tissue specimens. No pancreatic samples were excluded from experimentation/analyses unless otherwise stated in the manuscript (see Table 3). Mann-Whitney U test was used when the data were not normally distributed by Shapiro-Wilk normality test and were not at equal variance by F-test. When the normal distribution and equal variance were confirmed, Student's t test were used. Kruskal-Wallis test and post-hoc Dunn's multiple comparison test were used for comparisons of more than two groups. Analyses were performed with GraphPad Prism 6.0 (GraphPad Software, La Jolla, CA) software and IBM SPSS Statistics version 23 (IBM, Armonk, NY).